Sounding out the river: Seismic and hydroacoustic monitoring of bedload transport in an alluvial river

October 31, 2023

Bronwyn Matthews[1*] (Bronwyn.Matthews@ed.ac.uk), Mark Naylor[1] (mark.naylor@ed.ac.uk), Hugh Sinclair[1] (hugh.sinclar@ed.ac.uk), Andrew Black[2] (a.z.black@dundee.ac.uk), Richard Williams[3] (richard.williams@glasgow.ac.uk), Calum Cuthill[1,4] (calum.cuthill@glasgow.ac.uk), Matthew Gervais[1] (matt.gervais@ed.ac.uk), Michael Dietze[5,6] (mdietze@gfz-potsdam.de), Anna Smith[1] (annaem.smith@protonmail.com)

[1] School of GeoSciences, University of Edinburgh
[2]School of Humanities, Social Sciences and Law, University of Dundee
[3]School of Geographical & Earth Sciences, University of Glasgow
[4]School of Engineering, University of Glasgow
[5] Geographical Insitute, Georg-August University Göttingen
[6]Geomorphologie, GFZ Potsdam
[*]Correspondence to: Bronwyn Matthews, School of Geosciences,
University of Edinburgh, Edinburgh EH8 9XP, UK.
E-mail: Bronwyn.Matthews@ed.ac.uk
Twitter: @BronwynMay96

Acknowledgements

We would like to thank the Glenfeshie Estate and Wildland Scotland for their support to the project through access to the field site. Naylor, Sinclair, Black, Cuthill, Gervais and Williams were funded on this project using the NERC Funded Project "Sounding out the River: Monitoring the mobilisation and transport of bedload in mountain rivers" as part of the NERC Digital Environment Program with Grant number NE/T005920/1. Matthews is funded by an EPSRC studentship (EPSRC EP/T517884/1). Smith contributed to the project through their undergraduate research project.

Pre-print statement

This paper is a non-peer reviewed preprint submitted to EarthArXivarticle and has been submitted to Earth Surface Processes and Landforms (ESPL) for peer review.

Sounding out the river: Seismic and hydroacoustic monitoring of bedload transport in an alluvial river

October 31, 2023

Abstract

Seismological observations provide a non-invasive and continuous means of indirect measurement of fluvial bedload transport (i.e. the transport of coarse granular material, as a function of water depth, in rivers). However, a significant challenge remains in independently characterising the seismic signature of bedload transport from other sources, such as turbulence. Previous research suggested using the hysteresis relationship between water level and frequency-filtered seismic power spectrum as a diagnostic tool for identifying bedload transport. We present a unique dataset from an alluvial Scottish river, including seismic and hydroacoustic measurements, to analyse bedload transport during the three successive high flow events within a year. Examining data from successive events enabled us to evaluate the consistency of bedload transport thresholds and the influence of past transport events. Our findings reveal that bedload transport was observed in all three events, with the threshold for entrainment influenced by antecedent events. Following the largest of the three events the entrainment water level dropped by 20%, meaning it was easier to mobilise sediment. We also found that while hysteresis patterns observed in the seismic observations were linked to the size and timing of high flow events, they were not a necessary observation for bedload transport to have occurred. In fact, despite bedload transport occurring in all three events, hysteresis was only observed in the largest event suggesting that hysteresis alone is insufficient for identifying bedload transport. Our work suggests that there is a greater richness in the seismic data than has previously been identified and exploited, providing crucial information for effective river and land-use management in a changing climate with potentially impacted high flow events.

Keywords— river, bedload transport, entrainment threshold, fluvial geomorphology, environmental

seismology

1 Introduction

The interplay of climate change and intensified flooding events pose significant threats to both infrastructure and ecosystems in many areas across the world. Climate change has brought about an increased frequency and severity of floods in some climates, including in the UK, leading to increased transportation of sediments and debris by rivers. The transport of coarse gravelly bedload can have significant impacts on infrastructure such as bridges and dams, and profound ecological consequences, altering riverbed morphology, disturbing aquatic habitats and negatively impacting aquatic species (Turowski, Badoux, and D. Rickenmann, 2011; Roth, Finnegan, et al., 2017; Church, 2006). Additionally, anthropogenic activities, including urban development, deforestation, channelisation of rivers for river management, as well as re-naturalisation of rivers, alters the patterns of bedload transport in rivers (Cox et al., 2021). Therefore, being able to monitor and understand the timing and nature of coarse sediment mobilisation is important for predicting changes in channel morphology and is crucial for a range of applications, such as ensuring the robust design and maintenance of infrastructure against fluvial erosion, aiding in effective flood management and response, optimising sustainable use of water resources, and preserving the health of aquatic ecosystems.

The dynamic nature of sediment movement in river systems makes monitoring and measuring the transport of coarse bedload challenging, particularly as rivers erode, aggrade and shift their course. One of the key challenges lies in accurately measuring the onset of entrainment of bedload in the water column, and the mobilisation of larger-scale bedforms such as braid bars within channels. Variations in entrainment thresholds are widely recognised as being caused by processes such as particle shape and size distribution (P. R. Wilcock and Crowe, 2003; R. Jain, Tschisgale, and Fröhlich, 2021), bedforms (Church, Hassan, and Wolcott, 1998), sediment cohesion (Kothyari and R. K. Jain, 2008), and changes in grain size between the bed surface and subsurface where coarse sediment may act to armour the river bed (Lisle and Madej, 1992; R. Jain, Tschisgale, and Fröhlich, 2021). Using flume tank experiments it has been demonstrated that variations in these characteristics respond to durations and frequencies of moderate to peak discharge conditions (Ockelford, Woodcock, and Haynes, 2019; Luo et al., 2023). The grain-size distribution may be modified at the bed surface by winnowing of finer grains resulting in the formation of an armoured surface layer of coarser grains (Pitlick, Cui, and P. Wilcock, 2009; Gomez and Philip J. Soar, 2022). This armouring modifies the onset of bedload entrainment complicating the relationship between the measured grain-size distribution and the entrainment threshold. A further complication to the measurement of bedload transport are hysteresis patterns, where sediment transport rates do not have a linear scaling with the flow conditions (Bogen, 1980). Armouring is an example of a process that could result in hysteresis, as it can increase the threshold for sediment motion, modify the energy dissipation from the water, and influence sediment storage, resulting in different responses to rising and falling flow conditions. The mobilisation of coarse bedload can also be influenced by the volume of suspended sediment in the water column (Dieter Rickenmann, 1991; An et al., 2018), and due to a commonly observed prevalence of suspended loads during rising flow conditions compared to falling flow conditions, an asymmetry in bedload transport between the two phases can develop, resulting in hysteresis. Such non-linear and thresholded behaviour makes it difficult to predict the timings and intensity of bedload transport. Temporal variations in the bedload transport thresholds, in response to changes in near surface sediment characteristics have not been documented in alluvial rivers.

Addressing these challenges requires innovative site and reach-scale measurement techniques, geomorphological and hydrological field observations, and sediment transport modelling to gain a more comprehensive understanding of bedload transport dynamics, and the interplay between sediments, flow dynamics, and riverbed characteristics. However, since coarse bedload is mobilised when rivers are at high flow, logistical challenges are introduced when using many measurement techniques. Traditional methods of monitoring bedload transport in rivers, such as sediment sampling, sediment traps, grain size analysis and flow measurements, have typically relied on direct field measurements and observations. However, these approaches come with several limitations: sediment sampling and flow measurements can be labour-intensive, time-consuming, and difficult at high flows, while sediment traps (although continuous in measurement) are prone to errors due to bedload particles bouncing over or around the traps, and are subject to damage during high flows (Brasington, Langham, and B. Rumsby, 2003; Thorne, 2014; Bunte, Abt, et al., 2004; Bunte and Abt, 2005). These traditional methods struggle to capture the full complexity and natural dynamics of bedload transport, as they are typically performed during mild hydrologic events, over short timescales, and during daylight hours. As a result, they may not provide sufficiently representative data needed for effective river management, infrastructure design, or understanding sediment transport patterns. Engineers often use numerical models or empirical equations as alternatives to traditional methods for predicting bedload transport (Geay et al., 2020). However, simplification of these empirical equations relative to complexities of natural bedload transport processes in rivers, and the challenge of estimating grain size distribution, entrainment thresholds, and bed morphology among other factors, results in considerable uncertainties in the sediment transport predictions (Dey, 2014; Downs, P. J. Soar, and Taylor, 2016).

Modern technologies and advanced measurement techniques are increasingly being employed to address these limitations and provide more precise insights into bedload transport dynamics. Several recent studies have explored the potential for seismic sensors (such as geophones) to be used to monitor environmental and geomorphic processes (e.g. Roth, E. Brodsky, et al., 2016; Dietze and Gimbert, 2019; Burtin, Bollinger, et al., 2008; Lagarde et al., 2021). Geophones, which are typically used for seismic studies, have important applications in the field of bedload transport monitoring. Previously, geophones have been strategically deployed in riverbeds or on river banks to capture the ground vibrations caused by bedload particles interacting with the river bed. These vibrations can be analysed to estimate the timings, intensity and frequency of bedload transport in rivers. This innovative use of geophones provides a non-intrusive and continuous monitoring method that overcomes some limitations associated with traditional bedload measurement techniques, facilitating the monitoring of bedload transport under conditions that were previously not possible (Burtin, Vergne, et al., 2010). Geophones record a range of environmental signals that are filtered by their passage through the earth. The potential sources for these signals include precipitation, wind, tides, traffic, turbulent motion in rivers, and the impact of bedload on riverbeds (W. S. D. Wilcock, Webb, and Bjarnason, 1999; Burtin, Bollinger, et al., 2008; Rindraharisaona et al., 2022). Previous studies have focused on the frequency characteristics of seismic energy to discriminate different sources of seismic noise (Burtin, Bollinger, et al., 2008; Burtin, Hovius, et al., 2014; Gimbert, Tsai, and Lamb, 2014). The key discrimination for river induced seismic signals is between coarse bedload transport and water turbulence. It has been suggested that bedload transport induces broadband higher frequency seismic waves than the continuous signal from river turbulence (Schmandt et al., 2013; Gimbert, Tsai, and Lamb, 2014; Vore et al., 2019).

By correlating the bedload induced seismic data with river discharge, crucial insights have been gained into the dynamics of sediment transport and how it responds to variations in hydraulic characteristics. Many studies found a hysteretic relationship between these parameters which has been interpreted to be evidence of bedload transport, as significant hysteresis is not expected in the relationship between river stage and turbulence (Hsu, Finnegan, and E. E. Brodsky, 2011; Turowski, Böckli, et al., 2013; Roth, E. Brodsky, et al., 2016; Roth, Finnegan, et al., 2017). As outlined above, factors like particle size, shape and bed structure can influence the initiation of bedload transport on rivers, such that sediment entrainment thresholds may vary relative to changes in flow conditions. Bedload transport may even continue after water level has begun to decrease, or may initiate and cease at different levels, since it takes time for particles to be entrained or re-deposited based on the local hydraulic conditions. This interpretation of hysteresis has become a foundational assumption for many fluvial seismic studies, with some studies reporting a clockwise pattern of hysteresis where bedload transport peaks before the peak in water level, and some recording an anticlockwise pattern where the peak in water level occurs prior to the peak in bedload transport. Clockwise patterns are associated with readily available sediments (Reid, Frostick, and Layman, 1985; Kuhnle, 1992; Hassan, Egozi, and Parker, 2006; Gaeuman, 2010; L. Mao, 2012; Luca Mao et al., 2014), while anticlockwise patterns are thought to be caused by processes that increase sediment supply after a flood peak (Reid, Frostick, and Layman, 1985; Kuhnle, 1992; Lee, Liu, and Cheng, 2004; Luca Mao et al., 2014). These previous studies have shed light on the invaluable use of geophones for bedload monitoring purposes, however they generally had little independent data to constrain when bedload was being transported.

In order to test some of these assumptions used in interpreting geophone data, we combine geophones with hydrophones to independently classify when coarse bedload is transported. Hydrophones are typically used to detect and record underwater sound, making them particularly useful for applications in the fields of marine biology, underwater communication, and sonar systems (**ballance˙acoustic˙nodate**; Bountourakis, Elvander, and Pulkki, 2023). In contrast to geophones, hydrophones can record all particle collisions within the local river channel – collisions between particles and the bed as well as inter-particle collisions. However, it is more logistically difficult to deploy them routinely as they have to be placed within a rivers water column for the duration of the measurements, thus requiring careful methodological approach and appropriate housing to protect the instrument during high flow events. On an event-by-event basis they can provide independent data to critique the seismic bedload transport information obtained from geophones and to test whether hysteresis in the relationship between the fluvial seismic signal and water level is in fact a fingerprint of bedload transport.

Here, we use co-located hydrophones to test the application of geophones in characterising the onset of coarse bedload transport, and the presence of hysteresis during the passage of a flood hydrograph. Our study determines bedload mobilisation thresholds and evaluates the influence of antecedent events through independent seismic and hydroacoustic characterisations. By integrating seismic, water level, and hydroacoustic data we aim to gain insights into bedload transport thresholds, examine hysteresis patterns, and shed light on the intricate relationship between flowing water and sediment. Our analysis focuses on a relatively stable section of the gravel-bed River Feshie, in the Scottish Cairngorms (Figure 1) and analyses seismic signals from the three largest flow events in 2022. This enables the consistency of bedload transport entrainment thresholds to be examined and explored, and the effects of antecedent events on the thresholds observed. Our findings will contribute to more informed decision-making in river systems management and environmental protection, by constraining entrainment thresholds and hence enabling calculations and model predictions of sediment mobility in the channels.

2 Methods

2.1 Field site: River Feshie

The River Feshie, in Scotland, is an alluvial tributary of the River Spey and drains a catchment of $\sim 240\text{km}^2$ with maximum elevation of just over 1200 m (Figure 1) (Ferguson and Werritty, 1983). The bedrock has low permeability which results in a hydrograph that is very responsive to rain and snowmelt events (Chełmicki and Krzemień, 1999). The headwaters sit on the peat-rich plateau of the Cairngorms (upstream of SG1 in

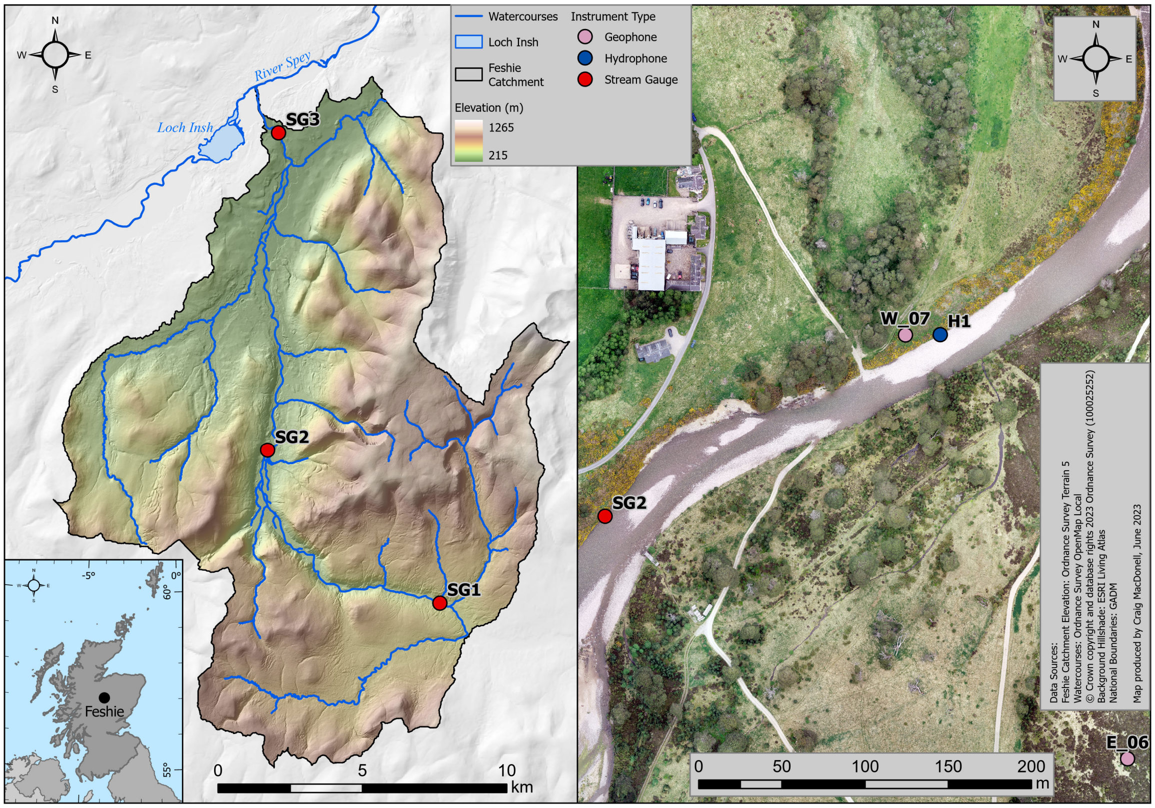

Figure 1: Maps of the River Feshie fieldsite at the (a) catchment scale showing the three stream gauge sites, (b) reach scale showing the sites of instruments used in this study, and (c) national scale. Photos of the field deployments can be found in Supplemental Material S1.

Figure 1) and then flow downstream through glacial outwash gravels (downstream of SG1 in Figure 1). The Feshie is supplied largely by the erosion of glacial moraine and outwash channels resulting in a broad, braided gravel-dominated river (Ferguson and Werritty, 1983; Brasington, B. T. Rumsby, and Mcvey, 2000). We focus on a 500m long, single thread reach just downstream of a wide multi-thread braided section (Figure 1 and 2). Within the study site, the channel width varies between 25 m to 70 m and has a local slope of ~ 0.006. The bedrock is predominantly Moinian schist and granite which dominate the bedload. The average grain sizes in the bar adjacent to the geophone station measured using the Wolman pebble count method (Wolman, 1954) routinely before and after the 2022 events are: $D_{16} = 14$ mm, $D_{50} = 35$ mm and $D_{84} = 72$ mm.

In the late 1970s a stream gauge was maintained in the same stretch as our study site by Ferguson and Werritty (1983) and recorded a mean flow of 3-4 m^3s^{-1} with regular floods reaching 20-30 m^3s^{-1} and the largest floods recorded exceeded 100 m^3s^{-1}. A stream gauge that is currently located approximately 12 km downstream at Feshiebridge (SG3), maintained by SEPA (Scottish Environment Protection Agency), reveals the same variable flow regime with peak flows exceeding 100 m^3s^{-1} and a maximum peak flow of 260

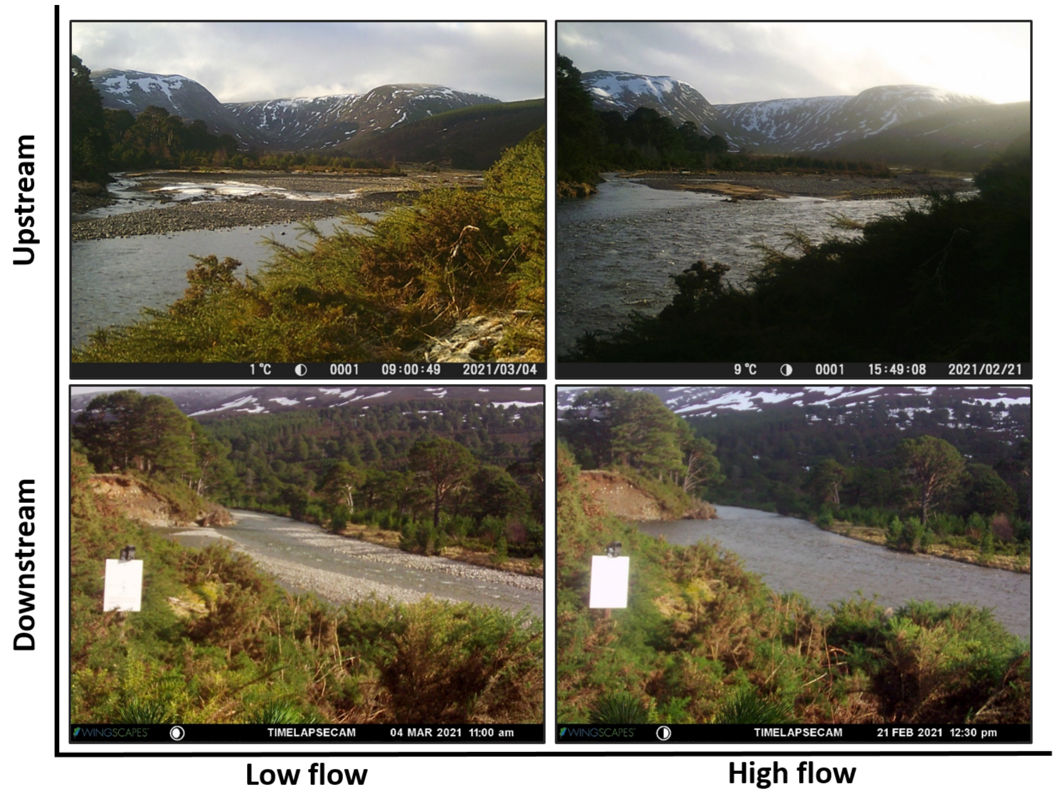

Figure 2: Photos from the River Feshie fieldsite looking upstream and downstream from SG2 during high flow and low flow levels. Images are taken from February and March 2021 as these had the clearest picture and are representative of general high and low flows at the site. During the low flow event the SEPA stream gauge at SG3 measured a water level of 0.76 m and the high flow event photographed here peaked at 2.15 m at SG3.

m^3s^{-1}. From flow data over the last 8 years at Feshiebridge (SG3) (Figure 3) it can be seen that there is a diurnal cycle with generally larger flows occurring during winter and spring. Flow patterns of 2022 were generally similar to previous years with low flows during summer and larger peaked flows in spring, autumn and winter. Summer flows in 2022 were particularly low, and were bounded by large events in early spring and autumn. The largest event of 2022, which we use for this analysis, peaked at around 138 m^3s^{-1}. Prior to this there had only been six other peaks that exceeded this level over the years plotted in Figure **??**, the largest of these occurring in December 2015 as a result of Storm Frank that caused widespread flooding across much of Scotland, Northern England and Wales (Barker et al., 2016).

2.2 Data collection

2.2.1 Stream Gauge Data

This study uses water level (stage) measurements recorded at three stream gauge sites on the River Feshie. To measure water level at our study site, we deployed a LiDAR (Light Detection and Ranging) water level

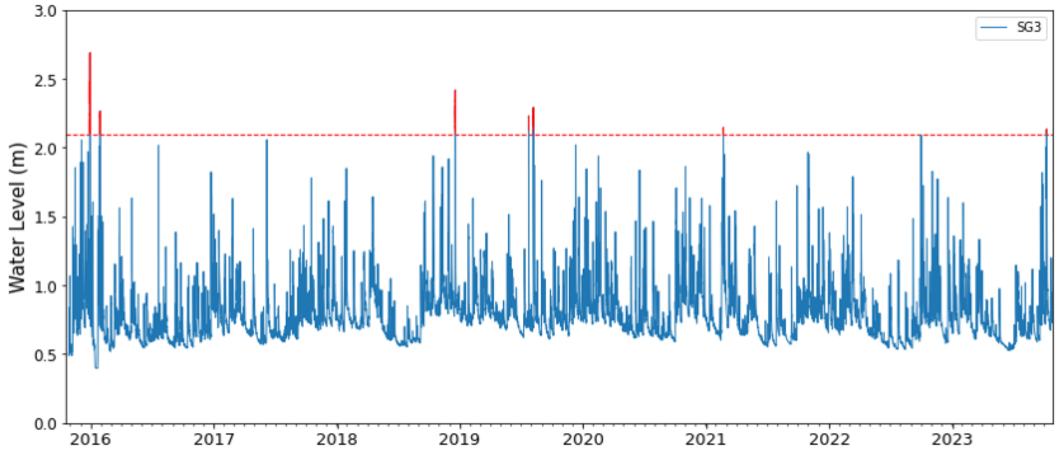

Figure 3: Stage measurements from SEPA stream gauge at SG3 over the last 8 years. Red stars mark the three largest events in 2022 that are analysed in this study. Red line marks the water level of the largest event in 2022, with peaks over the plotted record that have exceeded this value also marked in red.

sensor on the remains of a footbridge at site SG2 which takes repeat measurements of the distance to the water surface every 5 minutes. Using this data combined with channel geometry measurements, we have been able to convert to discharge values, however we will be using stage data in this analysis as it is more accurate measured data. We also have access to water level (stage) and discharge data collected every 15 minutes at stream gauges SG1 and SG3, located approximately 10km upstream and downstream of our site (Figure 1). These data are managed by Dr Andrew Black (Dundee University) and SEPA, respectively.

The three events analysed in this study occurred on the 11th - 14th March 2022 (three successive peaks with a maximum water level of 1.27 m at SG2), 30th September - 1st October 2022 (one peak with a maximum water level of 1.69 m at SG2, a one-in-eleven year event), and 2nd - 3rd November 2022 (one peak with a maximum water level of 1.30 m at SG2). These events are herein referred to as the 'March event', the 'September-October event', and the 'November event', respectively. The March event follows a series of snowmelt cycles that caused three repeated peaks in water level, resulting from rainfall on snow combined with snowmelt and reaches a peak discharge of 84 m^3s^{-1} at the SEPA station SG3. The larger September-October event is of a shorter duration and occurs following intense precipitation in the catchment that coincides with the tailend of Hurricane Fiona that hit Canada in mid-late September 2022, resulting in peak discharge of 131 m^3s^{-1} at SG3. The November event is an early winter storm with similar magnitude to the March event, however it occurs as a result of high rainfall alone, reaching peak discharge at 90 m^3s^{-1}. The three peaks in the first event allow us to test the consistency of the onset of bedload, the second event allows us to explore the impact of a large event on these thresholds of motion, and the final event allows us to explore the new behaviour of the river after a large event. Thus combining data from successive high flow events demonstrates how the technique can be used to make inferences about the effects of antecedent events on the mobilisation of bedload.

2.2.2 Seismic and Hydroacoustic Data

This study integrates seismic and hydroacoustic data to study the mobilisation and transport of bedload along a short (∼100 m) stretch of the River Feshie (Figure 1). We use the co-located stream gauge sensor (SG2) as a proxy for discharge.

We compare data from two 3-component PE6B (4.5Hz) geophones connected to Digos DataCube loggers recording at a sampling rate of 200 Hz. The geophone data is continuously recorded. The geophones are buried in soil at approximately 10 cm depth, levelled and oriented with the North-South (horizontal) component aligned along the downstream river direction. The geophone at site W_07 is located within 5m of the river and is well sited to record a strong river signal as the small source-to-sensor distance minimises the attenuation of high frequencies which is important for this study as we are wanting to resolve frequencies of bedload transport (Figure 1). The other geophone at site E_06 is located approximately 300m from the river as a control site to characterise other sources of environmental noise, such as precipitation and wind as the impact or rain on the ground and the movement of vegetation by wind can be recorded by geophones. Signals which are common to both W_07 and E_06 we identify as non-river environmental noise, and this approach allows us to confirm that the relatively high broadband noise level prior to the water rising is due to hydrometeorological noise. Generally, seismic bedload studies have used the vertical component of seismic waves as due to the impact direction of bedload on the river bed it was assumed that the emitted seismic waves would be best represented by Rayleigh waves with strong vertical displacements (Tsai et al., 2012; Dietze, Lagarde, et al., 2019). Here, we present the analysis of the stream-parallel component. This was chosen because, although using the vertical and the stream-perpendicular components for the analysis gave similar results, the vertical component tends to be noisier due to its susceptibility to rain interference (see Supplemental Material S2) and theoretically the stream-parallel component should give the strongest river-related signal. The area is anthropogenically very quiet with little traffic on the estate roads, and so there is minimal interference from these sources. The geophones are expected to record both the interaction of turbulence in the water with the bed and direct collisions of particles with the bed. It has previously been found that seismic waves emitted from bedload collisions resulted in higher frequencies than those from turbulence, with bedload generally found to occur in the range of 30-60 Hz and turbulence around 1-20 Hz (Tsai et al., 2012; Gimbert, Tsai, and Lamb, 2014; Dietze and Gimbert, 2019).

To independently characterise the bedload motion recorded within the study site, we deployed a hydrophone (Jez Riley French D-series) within the river at site H1 connected to our own Raspberry Pi logger, to record the hydroacoustic signal of turbulence and bedload motion. In previous hydroacoustic studies hydrophones have been deployed in metal pipes or attached to metal plates embedded in the river bed (Barrière et al., 2015), attached to the bottom of boats or river surveying equipment such as river boards (Geay et al., 2020), or attached to man-made infrastructure, such as bridges or metal frames (Belleudy, Valette, and Graff, 2010), however this was not an option in our study site. Instead, the hydrophone was mounted within a roughly 40 kg (0.4 m x 0.3 m x 0.3 m) granite block with a hollow cylindrical core of diameter 0.2 m in order to protect it from damage by direct impacts from mobile material (see Supplemental Material S1). The hydrophone block is located approximately 5 m downstream of the geophone at site W_07 and 40cm from the river bank (Figure 1). The recording system is built using a PiZero, a Witty Pi for scheduling and a HiFiBerry DAC+ADC Pro sound card (sampling at 44.1 kHz); due to the size of the datafiles, we record a 30 second sample every 15 minutes. Data are recorded at two different gains of 30 dB and 40 dB to manage potential issues of clipping and data quality. In addition to measuring collisions between particles and the bed like geophones, hydrophones also record collisions of particles in suspension. The hydroacoustic data is used as a complementary data set to the seismic data to confirm the occurrence and timing of bedload motion.

2.3 Data processing and analysis

We preprocess the seismic data by removing the instrument response and then detrend the data using ObsPy. Next, we generate a spectrogram, computed using Welch's method with a 1-minute window and no overlap, to quantify the variation in seismic power as a function of time and frequency, which we compare to water level. The resulting Power Spectral Density (PSD) reports power in each minute window as a function of frequency of the seismic waves. In order to isolate the bedload signal, the standard methodology is to then average the PSD over the relevant frequency bands (Tsai et al., 2012; Bakker et al., 2020; Lagarde et al., 2021). This frequency range is typically around 30-60 Hz with turbulence found to be approximately 1-20 Hz (Tsai et al., 2012; Gimbert, Tsai, and Lamb, 2014; Dietze and Gimbert, 2019). This approach allows us to compute the PSD for the seismic energy recorded within the frequency range commonly associated with the appearance of bedload transport.

The hydroacoustic data contains a lot of information about the processes occurring in the river. There is a distinct audible signal from turbulence (gurgling), smaller grain sizes being transported (tinkling and tapping), and larger grain sizes being transported (thudding and knocking), which can be used to manually classify the dominant process (see Audio 1-3). For the duration of each of the three high flow events considered here, the 30 second hydroacoustic recordings taken every 15 minutes were manually categorised by whether bedload was being transported and whether it was not. The recordings were categorised as 'Bedload Transport' if they were dominated by moving pebbles with $\sim$10 pebble hits over a 5 second window, however if there was only the occasional pebble movement (<10 per 5 seconds) and it was dominated by turbulence noises the files were classified as 'No Bedload Transport'. The categorisation into the larger and smaller grains being transported is a bit more ambiguous as it relied on an audible identification, however more work could be done to look at the frequency characteristics of the hydroacoustic data. The same researcher processed all the hydroacoustic data to minimise errors in the categorisation. At low water levels (~ 0.6 m) the hydrophones are exposed and therefore don't record any river related signals so are excluded from our analysis. This provides independent evidence of when bedload is being transported that we can overlay on the seismic analysis to test whether bedload transport and hysteresis in the PSD are directly related.

The water level data collected on-site was corrected for the height of the sensor above the riverbed to provide approximate water depth measurements, assuming the river bed was fixed. All stream gauge data, including that accessed from gauges SG1 and SG3, were interpolated and resampled to one-minute intervals so that they can be combined with the geophone data that was analysed in minute long windows. Since the water level hydrographs during a high flow event are fairly smooth it is easy to interpolate between the 15 minute samples. This also provided us much more richness in the data, as resampling the geophone data to 15 minute intervals to match the original stream gauge data would potentially miss important information from the propagating flood waves.

3 Results

The results compare the co-located geophone and hydrophone data at site W_07 and H1, respectively, and geophone data collected at a control site approximately 300 m away from the river (E_06). This comparative analysis is supported by locally measured stream gauge data from SG2 (Figure 1c). The results discuss the river-induced seismic signals at the two geophone sites, the observed transport thresholds over three successive high flow events, and the robustness of using hysteresis as a fingerprint of bedload transport.

3.1 Comparison of the river site with the non-fluvial control site

First we compare and contrast the geophone data recorded beside the river (W_07) and at the control site (E_06) in order to discriminate background environmental signals from those sourced from the river channel.

The water-level time series and spectrograms derived from the geophone data at each site are plotted in Figure 4 for two different events. The plots in each column have common time axes; the November event is not shown because the control site geophone E_06 was not recording at this time. Prior to the water rising, all the spectrograms show vertical broadband streaks of high amplitude (approximately -140 to -145 dB), which correspond to the periods of rain that necessarily precede the water level rising as we observed no snowmelt-only hydrological events (Figure 4 (c-f)). Similarly, when the water level is dropping, it is likely that there will be less rain at the site, and fewer vertical streaks on the spectrogram, as the water level would not be dropping if there was still significant rain across the catchment. This assumption does not necessarily hold true for large catchments as local conditions may vary from catchment wide conditions, such as rainfall patterns, however our interpretation makes this assumption due to the relatively small catchment size. Some of these streaky broadband signals could also be a result of wind but it is difficult to differentiate the two without further meteorological data as they tend to have similar characteristics and occupy similar frequency bands (Rindraharisaona et al., 2022).

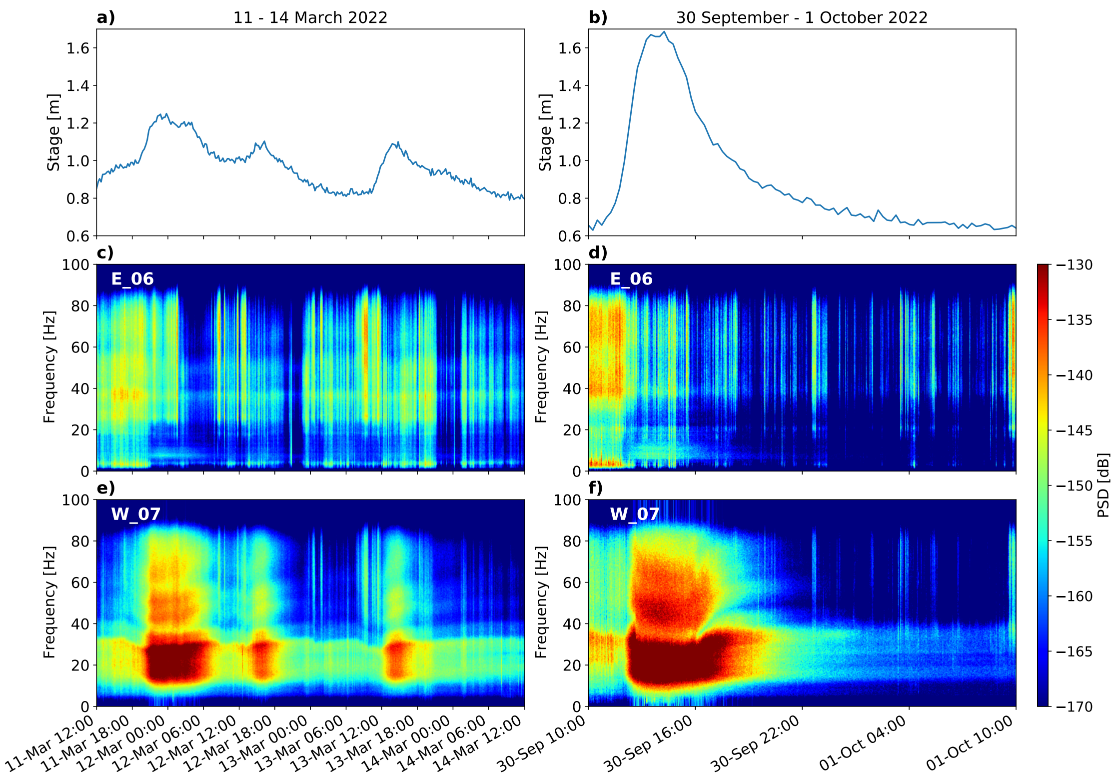

Figure 4: Data for two distinct high flow events in March and September-October 2022, one in each column. Included in this plot are; (a, b) the time-series of the water level at SG2, (c, d) the spectrograms of the geophone data (in 1 minute windows) at the control site to highlight environmental noise such as wind and rain, and (e, f) the spectrograms of the geophones at the river site which is dominated by signals of turbulence and sediment transport.

In contrast to the control site we see that the PSD time-series measured at the river bank station, W_07, evolves as the water level changes. During periods of base level flow, when the water is low, the greatest power is recorded within a frequency range of approximately 5-35 Hz and is continuous which suggests this is the background river signal (turbulence); this feature is absent at the control site. This value is slightly higher than those found in previous studies (as previously discussed) but is most likely a result of site characteristics. The sudden onset of higher frequency (30-80 Hz) high power seismic signals at W_07 recorded during the peak of the flood waves suggests that there is a separate signal in addition to that derived from turbulence. During the highest water levels, these high power bands extend to higher frequencies, up to around 85 Hz, but once the river level drops back down towards base levels these higher frequency signals become less dominant. These high power, high frequency signals are also absent from the control site, thus enforcing the interpretation that these are river related signals, but the hydroacoustic data will help clarify. These comparisons allow us to identify the seismic signals that are induced by river-related processes, and specifically those induced by bedload transport, which are then used throughout the rest of this study to analyse transport thresholds and patterns.

3.2 Analysis across three successive high flow events

Having documented the fingerprints of different physical processes within the time-frequency domain (Figure 4), we simplify the analysis by focusing on the 30-80 Hz band, as previous studies (e.g. Burtin, Bollinger, et al., 2008; Roth, E. Brodsky, et al., 2016; Turowski, Wyss, and Beer, 2015) have found that bedload transport occurs at higher frequencies than turbulence, which going by our interpretation from Figure 4 would be >30 Hz. Specifically, in minute long windows shown in the spectrogram, we average the values of the power over the 50 to 60 Hz range for three distinct high flow events to calculate a single scalar value at each time, which we refer to as the average power spectral density (aPSD) in the coming plots (See Section 2). This narrower frequency range was chosen as there was less influence from meteorological and turbulence seismic signals, making the bedload transport the strongest signal observed for those frequencies.

The aPSDs calculated using the selected frequency band of 50-60 Hz emphasise the use of site E_06 as a control site and the strength of the river-induced seismic signals recorded at W_07. At the control site the PSD is dominated by the contributions from the broadband intermittent meteorological (wind and rain) signal, aside from the reasonable likelihood that it has been raining in the vicinity before the water level rises. Consequently the aPSD shows a large amount of scatter that is independent of the water level (Figure 5 a,b). In contrast, the aPSD at the site beside the river, W_07, mirrors the variations in water level for all three events, showing a close parallel between the two (Figure 5 c-e). The meteorological noise is still visible at site W_07 prior to the hydrological peaks, but the river-induced seismic noise is dominant above base water levels as turbulence increases and bedload begins to mobilise.

3.2.1 Entrainment thresholds of coarse bedload

Using the hydrophone data, we classify whether bedload is being transported, independently of the geophone data, and include this information on the water-level versus aPSD plot (shaded regions in Figure 5 c-e, with white regions when the hydrophone was exposed out the water). All three of the high flow events resulted in the mobilisation of bedload during the peaks in water level. During the largest of the three events (the

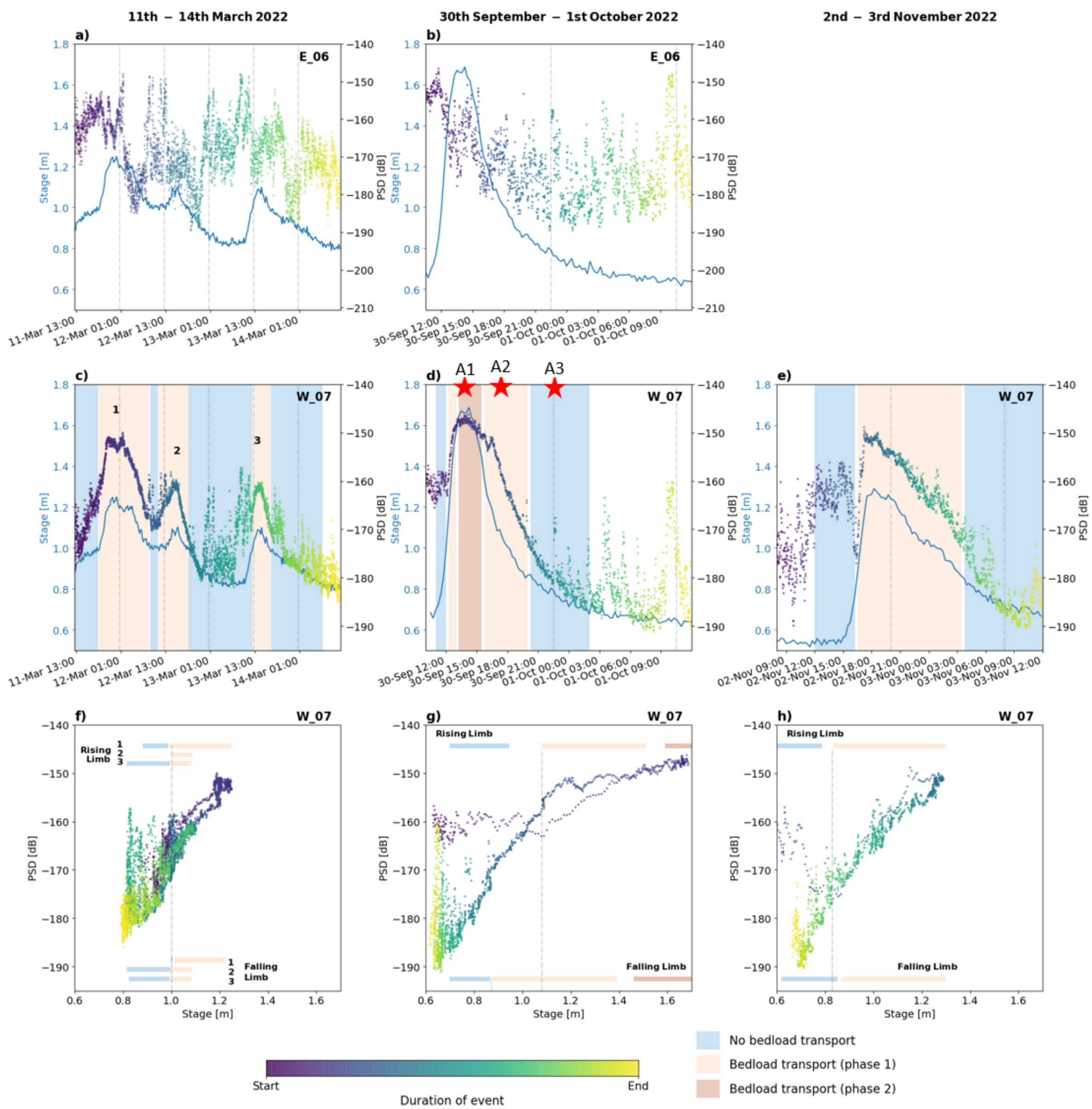

Figure 5: Plots summarising the time series of the water level (blue line) and seismic power averaged over the frequency range 50-60 Hz (points coloured by time) for the three largest flow events in 2022. Each column displays a different event showing; (a, b) the aPSD and water level timeseries' for the control site highlighting the environmental noise around the water level peaks, (c, d, e) the aPSD timeseries for the river site layered on top of the independent classification of bedload transport activity using the hydroacoustic data (blue shading shows periods where the hydrophone records only turbulence, salmon shows when bedload transport starts (phase 1) and red shows when there is an audible shift to lower frequencies on the hydrophone during bedload transport (phase 2)), (f, g, h) the PSD versus stage relationship with the hydrophone bedload transport classifications shown as bars for the rising and falling limbs of the hydrological peaks. Red stars in d) show the timings of the hydrophone recordings included in Audio 1-3.

September-October event) there was also an audible shift in frequency of the recording at the highest water level (¿ 1.60 m), which is shown in the reddish colour in Figure 5d at the peak of the event, which lasted approximately 135 minutes. Recordings during the two transport phases and the turbulence phase (Audio 1-3) highlight the audible changes during these processes. This audible frequency drop in the hydroacoustic data coincides with a shift to lower frequencies in the geophone data seen in Figure 4f and Supplemental Material S2, where the lower end of the high amplitude seismic power dips from about 40 Hz to around 30 Hz at the same time as the peak of the hydrograph and then rises back up following the peak. The gaps between the hydroacoustic categorisations in Figure 5 c-h are due to the 15 minute hydroacoustic sampling interval resulting in an uncertainty in the water level at which mobilisation of coarse bedload starts. Here, this water level uncertainty is greater during the rising limb than the falling limb (Figure 5f-h) due to the rapid rate of change in water level relative to the quarter-hourly hydrophone recordings. Similar features would be observed in a rapidly decreasing flow, however this was not the case in the events analysed here.

Further, we can compare the timing of onset of bedload transport with the water level at that time to explore any systematic changes in the threshold for motion and arrest across the three events. Figures 5 and 6 reveal that bedload mobilisation during the moderate scale March event consistently starts and stops at a water level of $\sim$1.00 m. This is the case across all three daily peaks, labelled 1-3 in Figure 5c. However, during the largest September-October event it is observed that coarse bedload transport initiates at between 0.95 m and 1.08 m, accounting for the uncertainty in the sampling period of the hydroacoustic data. The previously mentioned audible drop in frequency of the hydroacoustic data occurs between 1.50 m and 1.59 m and continues throughout the peak (at 1.69 m) and falling limb and stops at around 1.39 - 1.44 m, labelled 'Bedload transport (phase 2)' in Figure 5 and 6. At this point on the falling limb the audible frequency increases to similar to the initial mobilisation and bedload transport is sustained until the water level drops to $\sim$0.87 m. The September-October event therefore had coarse bedload mobilisation initiating at $\sim$1.00 m on the rising limb and ceasing at $\sim$0.87 m on the falling limb. The third event in November is much like the early March event in that the mobilisation of bedload starts and stops at the same level on the rising and falling limb of the hydrograph. However, for this event the entrainment threshold is now followed through from the September event at $\sim$ 0.79 - 0.87 m.

3.2.2 Hysteresis as a fingerprint of bedload transport

Now consider the water-level versus aPSD plots in Figure 5 f-h and Figure 6a. These allows us to test the validity of the assumption that hysteresis in the water level versus PSD is a reliable fingerprint of bedload transport. As noted above, bedload transport occurred during all three events which was evidenced through the hydroacoustic data. Looking at the water level versus aPSD plots it is clear that both the March and November events have relatively linear relationships and show no signs of hysteresis despite independent evidence from the hydroacoustic data that bedload was actively being transported. They also show very similar gradients of aPSD against water level for both the rising and falling limbs, suggesting that the nature of coarse bedload transport is similar for both events. In contrast, the aPSD analysed over the 50-60Hz range in the larger September-October event does exhibit some anticlockwise hysteresis, but only between ~ 1.00 m and 1.40 m. In addition the slope of the aPSD versus water level is lower at higher water levels (Figure 5g). Until around 12:00 on the 30th September (at water levels ¡ 1.00 m), the aPSD is relatively constant at around -160 dB for this event whilst the precipitation dominates the signal, as evidenced in Figure 5 d and discussed above. Once the water level reaches ∼1.00-1.10 m, the aPSD starts to rise at a similar gradient to the other two events but at slightly lower values of aPSD (Figure 5f and h; Figure 6). This occurs at a very similar entrainment threshold to what was observed through the hydroacoustic data, discussed above. At around 1.40 m the aPSD has risen to approximately -148 dB, and now levels off slightly. One possible cause for a levelling off like this could be due clipping of the waveforms when the recorded signal exceeds the upper limit of the geophones recording range, however this is not the case here and the observed behaviour is real (See Supplemental Material S3). This much lower gradient is sustained up to the peak of the event and continues with the falling limb until ∼1.15 m, at which point the gradient returns similar to the original gradient. This sustained lower gradient last longer on the falling limb than the rising limb, which can also be seen on the aPSD timeseries in Figure 5d where the aPSD remains close to peak levels for a short time after the peak even once the water level has begun to decrease.

In summary, the initial entrainment threshold that was observed in March 2022 dropped by about 15-20% (∼1.00 m to ∼ 0.80-0.85 m) following the September-October event peak and this new lower threshold was maintained for the subsequent November high flow event. The March and November events show no hysteresis whereas the larger September-October event shows a degree of anticlockwise hysteresis for water levels between ∼ 1.00 m and 1.40 m (when bedload transport is observed to initiate), and then behaves linearly at water levels above 1.40 m. Unfortunately, due to the noise from meteorological signals at the initial stages of the high flow events, it is difficult to identify any features in the seismic data that would indicate the initial transport of the coarse bedload, which is why the hydroacoustic data has proven very useful in this analysis.

4 Discussion

From seismic and hydroacoustic measurements at our field site in the alluvial River Feshie, it is clear that we can record information on the mobilisation of coarse bedload. One key finding we observe is that the coarse bedload transport threshold, and hence bed strength, depends on the recent history of larger discharge events. We believe that the largest event observed in 2022 leaves disordered material on the surface of the bed that is easier to re-mobilise than it was prior to the large event (R. Jain, Tschisgale, and Fröhlich, 2021).

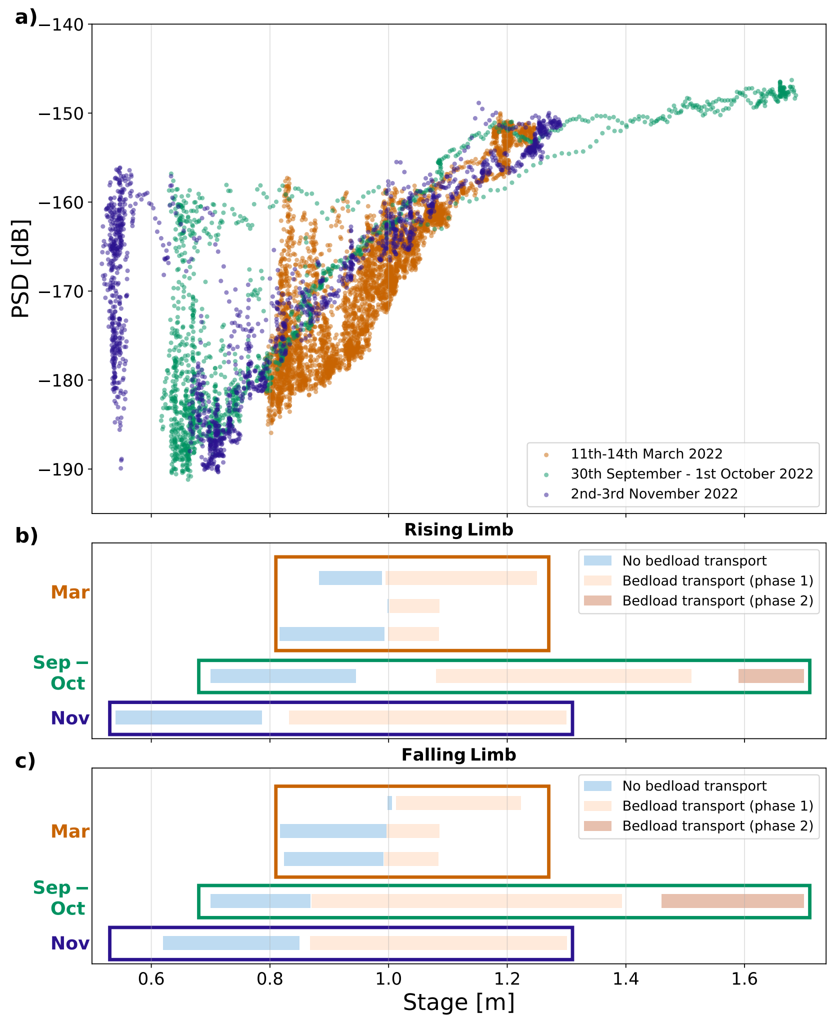

Figure 6: (a) Superposition of the PSD versus water level relationships for three distinct high flow events to enable a clearer comparison of the similarities and differences between each event. (b) Bedload activity transitions from independent interpretation of hydroacoustic data that occurred on the rising limbs of flood peaks for all three events; note that for the March and September events bedload started being transported at a water level of ~1.00-1.10 m whilst transport during the November event initiated at a water level of ~0.80 m. (c) Bedload activity transitions from independent interpretation of hydroacoustic data that occurred on the falling limbs flood peaks for all three events; note that for the March event bedload stopped being transported at a water level of ~1.00 m whilst the arrest of bedload transport occurred at ~0.85 m for the September and November events.

It was observed during routine field visits that the grain size distribution was not sorted before nor after the event. We therefore interpret the change in entrainment threshold as a consequence of changes in the grain structure and sorting on the river bed (R. Jain, Tschisgale, and Fröhlich, 2021) with greater deposition of unsorted material; this is consistent with the very rapid fall in water level inhibiting the bed to find a stable form (Luo et al., 2023). From drone surveys of the area in June and November 2022 it was also observed that there was no significant change to the width of the channel or the elevation of the bed, thus supporting our points above. The entrainment threshold changed by ~15 cm but the bed elevation did not change by this amount, therefore this is unlikely to have had an effect on the thresholds observed. We hypothesise that, in the absence of a further large flow event like the September-October 2022 event, over cycles of moderate scale events, such as snow melt cycles or moderate rainfall events like the March and November events, the bed will progressively regain its strength as the clasts locally reorganise and the water level threshold for mobility will again rise to a higher value (Ockelford, Woodcock, and Haynes, 2019; Luo et al., 2023). This hypothesis is supported by the observation that in the initial March event, the daily rainfall plus snowmelt cycles were just sufficient to initiate the motion of bedload at their peak suggesting that these moderate events have helped the system find a more stable configuration over time. Since events of a similar size to the March and November events are expected to happen approximately once every 10 months, the river will undergo frequent local sorting of material before a large one in 11 year event like September-October event breaks through the sorted material and causes large amounts of resorting.

Prior to this study, hysteresis in the water-level versus seismic PSD plot was viewed as a digital fingerprint for bedload transport (Burtin, Bollinger, et al., 2008; Hsu, Finnegan, and E. E. Brodsky, 2011; Roth, E. Brodsky, et al., 2016; Turowski, Wyss, and Beer, 2015). In our study bedload was transported in all three events, but hysteresis in the high frequency signal only occurred in the largest event when using co-located stream gauge data from SG2; thus using hysteresis alone as an indicator of bedload transport is insufficient to detect transport events. In our field site, as a conservative estimate, we saw hysteresis emerge for high flow events which exceeded water levels in excess of 1.30 m whilst the actual bedload mobilisation threshold varied between 0.85 m-1.00 m. We also see a levelling off of the PSD for water levels above 1.40 m which we interpret to be most likely caused by the presence of a sheet flow of granular material, which would make it difficult to increase the frequency and magnitude of collisions with the bed(Palucis et al., 2018), thus reducing the seismic power measured in the high frequencies with increasing water level. We believe that although there will be a limit on the grain-to-bed interactions during granular sheet flow, there will likely be increased grain-to-grain interaction which is possible to record with the hydroacoustics. Further analysis into the frequency characteristics of hydroacoustic data would potentially shed some light on this. However, under this scenario, due to the reduced grain-to-bed interactions, measurable with geophones, studies which attempt a mass balance based on hysteresis are likely to underestimate the total bedload transported (e.g. Chao et al., 2015) and the construction of a mass balance using geophones alone will struggle at high flow rates; a proper analysis of bedload flux will need to consider such non-linearity.

In conjunction with the expected hysteresis at high frequencies, previous studies have suggested that analysing the low frequency band ($<\sim$1-30 Hz, e.g. Dietze and Gimbert, 2019; Chao et al., 2015; Burtin, Bollinger, et al., 2008) can effectively isolate the turbulence signal. By focusing on this frequency range, it was believed that hysteresis would not be observed in the water-level versus PSD plot (Tsai et al., 2012).

However, findings from this study challenge these assumptions, especially in relation to the largest event analysed. Contrary to expectations, hysteresis is also observed in the lower frequency range, as shown in Supplemental Material S4. This adds complexity to distinguishing between turbulence and bedload seismic signals, potentially leading to inaccurate estimations of bedload transport fluxes. However, this analysis may be complicated by the fact that bedload and turbulence can occupy overlapping frequency ranges, and therefore discrimination of the frequency bands of interest is very important to avoid contamination of the data.

Looking forwards, long-term monitoring on this reach will allow us to observe a series of successive events with varying durations. This will provide us with a more comprehensive understanding of the factors influencing the threshold for bedload mobilisation. In particular, we can assess whether the bedload mobilisation threshold is primarily influenced by the magnitude of high flow events, the duration of individual events or the periods between events. Furthermore, we can explore the relationship between these dynamics, the arrangement of the riverbed structure, and the calculation of the entrainment threshold parameter, Shields stress.

5 Conclusions

Developing a clear, robust methodology for understanding and digitally monitoring bedload transport and fluxes is fundamental for informing engineering and flood risk models, particularly with the concerns regarding the increased extreme event occurrence as a result of climate change. The use of seismic sensors is a key step forward and provides the opportunity to monitor bedload transport in previously inaccessible conditions, however it is clear that care has to be taken when developing the methodological design. Combining seismic data with other measurement techniques such as hydroacoustic data, as done in this study, allows the independent interpretation of the mobilisation of bedload which can inform a more accurate analysis of the seismic signal from bedload transport. By studying three successive high flow events, we test for variations in the flow conditions in an alluvial river that characterise the onset and termination of particle entrainment, thereby exploring the presence of hysteresis in seismic data as a fingerprint of coarse bedload transport. Through the use of hydroacoustic data to independently characterise bedload transport, our study reveals that while hysteresis in seismic data, in relation to water level, can sometimes be indicative of bedload transport, it is not a definitive requirement. These findings emphasise the need to enhance our understanding of the factors that influence the occurrence of bedload transport, particularly in climate change-affected rivers. Being able to accurately distinguish between distinct seismic signals associated with bedload transport and water turbulence is crucial, and will enable us to improve our ability to estimate bedload transport fluxes and gain deeper insights into the complex dynamics of alluvial rivers impacted by climate change. Our study shows the value in combining seismic and hydroacoustic data for long-term digital monitoring of bedload transport and suggests the possibility that this combination of data will allow us to identify different granular flow regimes in the field. Routine monitoring with such digital systems enables us to understand the systematic evolution in the onset of bedload transport and will be of direct use in calibrating widely used flood and bedload transport engineering models.

References

Chenge An et al. “Can magic sand cause massive degradation of a gravel-bed river at the decadal scale? Shi-ting River, China”. In: *Geomorphology* 327 (Oct. 2018). DOI: 10.1016/j.geomorph.2018.10.026.

M. Bakker et al. “Field Application and Validation of a Seismic Bedload Transport Model”. en. In: *Journal of Geophysical Research* (2020), p. 22.

Lucy Barker et al. “The winter 2015/2016 floods in the UK: a hydrological appraisal”. en. In: *Weather* 71.12 (2016). _eprint: https://onlinelibrary.wiley.com/doi/pdf/10.1002/wea.2822, pp. 324–333. ISSN: 1477-8696. DOI: 10.1002/wea.2822. URL: https://onlinelibrary.wiley.com/doi/abs/10.1002/wea.2822 (visited on 10/20/2023).

J. Barrière et al. “Bed load transport monitoring using seismic observations in a low-gradient rural gravel bed stream: Seismic monitoring of bedload transport”. en. In: *Geophysical Research Letters* 42.7 (Apr. 2015), pp. 2294–2301. ISSN: 00948276. DOI: 10.1002/2015GL063630. URL: http://doi.wiley.com/10.1002/2015GL063630 (visited on 10/28/2020).

Philippe Belleudy, Alexandre Valette, and Benjamin Graff. “Monitoring of bedload in river beds with an hydrophone: first trials of signal analyses”. en. In: *Dittrich, Andreas; Koll, Katinka; Aberle, Jochen; Geisenhainer, Peter (Hg.): River Flow 2010* (2010). URL: https://hdl.handle.net/20.500.11970/99836.

J. Bogen. “The hysteresis effect of sediment transport systems”. en. In: *Norsk Geografisk Tidsskrift - Norwegian Journal of Geography* 34.1 (Jan. 1980), pp. 45–54. ISSN: 0029-1951, 1502-5292. DOI: 10.1080/00291958008545338. URL: http://www.tandfonline.com/doi/abs/10.1080/00291958008545338 (visited on 11/16/2020).

Vasileios Bountourakis, Filip Elvander, and Ville Pulkki. *Using optimal mass transport in bearing-time records for underwater target localization and tracking.* June 2023.

J. Brasington, J. Langham, and B. Rumsby. “Methodological sensitivity of morphometric estimates of coarse fluvial sediment transport”. en. In: *Geomorphology* 53.3 (July 2003), pp. 299–316. ISSN: 0169-555X. DOI: 10.1016/S0169-555X(02)00320-3. URL: https://www.sciencedirect.com/science/article/pii/S0169555X02003203 (visited on 02/01/2023).

J. Brasington, B. T. Rumsby, and R. A. Mcvey. "Monitoring and modelling morphological change in a braided gravel-bed river using high resolution GPS-based survey". en. In: (2000), p. 18.

Kristin Bunte and Steven R. Abt. "Effect of sampling time on measured gravel bed load transport rates in a coarse-bedded stream". In: *Water Resources Research* 41.11 (2005). DOI: https://doi.org/10.1029/2004WR003880. URL: https://agupubs.onlinelibrary.wiley.com/doi/10.1029/2004wr003880 (visited on 10/30/2023).

Kristin Bunte, Steven R. Abt, et al. "Measurement of Coarse Gravel and Cobble Transport Using Portable Bedload Traps". EN. In: *Journal of Hydraulic Engineering* 130.9 (Sept. 2004). Publisher: American Society of Civil Engineers, pp. 879–893. ISSN: 0733-9429. DOI: 10.1061/(ASCE)0733-9429(2004)130:9(879). URL: https://ascelibrary.org/doi/10.1061/%28ASCE%290733-9429%282004%29130%3A9%28879%29 (visited on 10/30/2023).

A. Burtin, L. Bollinger, et al. "Spectral analysis of seismic noise induced by rivers: A new tool to monitor spatiotemporal changes in stream hydrodynamics". en. In: *Journal of Geophysical Research* 113.B5 (May 2008). ISSN: 0148-0227. DOI: 10.1029/2007JB005034. URL: http://doi.wiley.com/10.1029/2007JB005034 (visited on 10/28/2020).

A. Burtin, N. Hovius, et al. "Seismic constraints on dynamic links between geomorphic processes and routing of sediment in a steep mountain catchment". en. In: *Earth Surface Dynamics* 2.1 (Jan. 2014), pp. 21–33. ISSN: 2196-632X. DOI: 10.5194/esurf-2-21-2014. URL: https://esurf.copernicus.org/articles/2/21/2014/ (visited on 10/28/2020).

A. Burtin, J. Vergne, et al. "Location of river-induced seismic signal from noise correlation functions: Location of river seismic signal". en. In: *Geophysical Journal International* 182.3 (Sept. 2010), pp. 1161–1173. ISSN: 0956540X. DOI: 10.1111/j.1365-246X.2010.04701.x. URL: https://academic.oup.com/gji/article-lookup/doi/10.1111/j.1365-246X.2010.04701.x (visited on 10/28/2020).

W.-A. Chao et al. "Seismologically determined bedload flux during the typhoon season". en. In: *Scientific Reports* 5.1 (July 2015), p. 8261. ISSN: 2045-2322. DOI: 10.1038/srep08261. URL: http://www.nature.com/articles/srep08261 (visited on 10/28/2020).

W. Chełmicki and K. Krzemień. “Channel Typology for the River Feshie in the Cairngorm Mts, Scotland”. en. In: *Prace Geograficzne* (1999), p. 12.

M. Church. “Bed Material Transport and the Morphology of Alluvial River Channels”. In: *Annual Review of Earth and Planetary Sciences* 34.1 (2006), pp. 325–354. DOI: 10.1146/annurev.earth.33.092203.122721. URL: https://doi.org/10.1146/annurev.earth.33.092203.122721 (visited on 04/12/2021).

M. Church, M. A. Hassan, and J. F. Wolcott. “Stabilizing self-organized structures in gravel-bed stream channels: Field and experimental observations”. en. In: *Water Resources Research* 34.11 (1998). _eprint: https://onlinelibrary.wiley.com/doi/pdf/10.1029/98WR00484, pp. 3169–3179. ISSN: 1944-7973. DOI: 10.1029/98WR00484. URL: https://onlinelibrary.wiley.com/doi/abs/10.1029/98WR00484 (visited on 03/10/2023).

J. R. Cox et al. “Anthropogenic Effects on the Contemporary Sediment Budget of the Lower Rhine-Meuse Delta Channel Network”. en. In: *Earth’s Future* 9.7 (2021). _eprint: https://onlinelibrary.wiley.com/ e2020EF001869. ISSN: 2328-4277. DOI: 10.1029/2020EF001869. URL: https://onlinelibrary.wiley.com/doi/abs/10.1029/2020EF001869 (visited on 10/30/2023).

S. Dey. *Fluvial Hydrodynamics*. en. GeoPlanet: Earth and Planetary Sciences. Berlin, Heidelberg: Springer Berlin Heidelberg, 2014. ISBN: 978-3-642-19061-2 978-3-642-19062-9. DOI: 10.1007/978-3-642-19062-9. URL: http://link.springer.com/10.1007/978-3-642-19062-9 (visited on 11/20/2020).

M. Dietze and F. Gimbert. “The seismic view on sediment laden ephemeral flows – modelling of ground motion data for fluid and bedload dynamics in the Arroyo de los Piños”. en. In: (2019), p. 10.

M. Dietze, S. Lagarde, et al. “Joint Sensing of Bedload Flux and Water Depth by Seismic Data Inversion”. en. In: *Water Resources Research* 55.11 (2019), pp. 9892–9904. ISSN: 1944-7973. DOI: https://doi.org/10.1029/2019WR026072. URL: https://agupubs.onlinelibrary.wiley.com/doi/abs/10.1029/2019WR026072 (visited on 02/26/2021).

P. W. Downs, P. J. Soar, and A. Taylor. “The anatomy of effective discharge: the dynamics of coarse sediment transport revealed using continuous bedload monitoring in a gravel-bed river during a very wet year: Dynamics of coarse sediment transport using continuous monitoring". en. In: *Earth Surface Processes and Landforms* 41.2 (Feb. 2016), pp. 147–161. ISSN: 01979337. DOI: 10.1002/esp.3785. URL: http://doi.wiley.com/10.1002/esp.3785 (visited on 10/28/2020).

R. I. Ferguson and A. Werritty. "Bar Development and Channel Changes in the Gravelly River Feshie, Scotland". en. In: *Modern and Ancient Fluvial Systems*. Ed. by J. D. Collinson and J. Lewin. Oxford, UK: Blackwell Publishing Ltd., Feb. 1983, pp. 181–193. ISBN: 978-1-4443-0377-3 978-0-632-00997-8. DOI: 10.1002/9781444303773.ch14. URL: http://doi.wiley.com/10.1002/9781444303773.ch14 (visited on 10/28/2020).

D. Gaeuman. "Mechanics of Bedload Rating Curve Shifts and Bedload Hysteresis in the Trinity River, California". en. In: (2010).

T. Geay et al. "Passive Acoustic Measurement of Bedload Transport: Toward a Global Calibration Curve?" en. In: *Journal of Geophysical Research: Earth Surface* 125.8 (2020). _eprint: https://onlinelibrary.wiley.com/doi/pdf/10.1029/2019JF005242, e2019JF005242. ISSN: 2169-9011. DOI: 10.1029/2019JF005242. URL: https://onlinelibrary.wiley.com/doi/abs/10.1029/2019JF005242 (visited on 01/13/2022).

F. Gimbert, V. C. Tsai, and M. P. Lamb. "A physical model for seismic noise generation by turbulent flow in rivers". en. In: *Journal of Geophysical Research: Earth Surface* 119.10 (Oct. 2014), pp. 2209–2238. ISSN: 21699003. DOI: 10.1002/2014JF003201. URL: http://doi.wiley.com/10.1002/2014JF003201 (visited on 10/28/2020).

Basil Gomez and Philip J. Soar. "Bedload transport: beyond intractability". In: *Royal Society Open Science* 9.3 (Mar. 2022). Publisher: Royal Society, p. 211932. DOI: 10.1098/rsos.211932. URL: https://royalsocietypublishing.org/doi/10.1098/rsos.211932 (visited on 10/30/2023).

M. A. Hassan, R. Egozi, and G. Parker. "Experiments on the effect of hydrograph characteristics on vertical grain sorting in gravel bed rivers". en. In: *Water Resources Research* 42.9 (2006). ISSN: 1944-7973. DOI: https://doi.org/10.1029/2005WR004707. URL: https://agupubs.onlinelibrary.wiley.com/doi/abs/10.1029/2005WR004707 (visited on 12/03/2020).

L. Hsu, N. J. Finnegan, and E. E. Brodsky. "A seismic signature of river bedload transport during storm events". en. In: *Geophysical Research Letters* 38.13 (July 2011). ISSN: 00948276. DOI: 10.1029/2011GL047759. URL: http://doi.wiley.com/10.1029/2011GL047759 (visited on 10/28/2020).

R. Jain, S. Tschisgale, and J. Fröhlich. "Impact of shape: DNS of sediment transport with non-spherical particles". en. In: *Journal of Fluid Mechanics* 916 (June 2021). Publisher: Cambridge University Press, A38. ISSN: 0022-1120, 1469-7645. DOI: 10.1017/jfm.2021.214. URL: https://www.cambridge.org/core/journals/journal-of-fluid-mechanics/article/impact-of-shape-dns-of-sediment-transport-with-nonspherical-particles/0B3ED0C2B19C84AB97EB83F7362389A8 (visited on 05/31/2023).

U. C. Kothyari and R. K. Jain. "Influence of cohesion on the incipient motion condition of sediment mixtures". en. In: *Water Resources Research* 44.4 (2008). ISSN: 1944-7973. DOI: 10.1029/2007WR006326. URL: https://onlinelibrary.wiley.com/doi/abs/10.1029/2007WR006326 (visited on 03/10/2023).

R. A. Kuhnle. "Bed load transport during rising and falling stages on two small streams". en. In: *Earth Surface Processes and Landforms* 17.2 (1992), pp. 191–197. ISSN: 1096-9837. DOI: https://doi.org/10.1002/esp.3290170206. URL: https://onlinelibrary.wiley.com/doi/abs/10.1002/esp.3290170206 (visited on 12/03/2020).

S. Lagarde et al. "Grain-Size Distribution and Propagation Effects on Seismic Signals Generated by Bedload Transport". en. In: *Water Resources Research* 57.4 (2021). ISSN: 1944-7973. DOI: https://doi.org/10.1029/2020WR028700. URL: https://agupubs.onlinelibrary.wiley.com/doi/abs/10.1029/2020WR028700 (visited on 05/31/2021).

K. T. Lee, Yi-Liang Liu, and Kai-Hung Cheng. "Experimental investigation of bedload transport processes under unsteady flow conditions". en. In: *Hydrological Processes* 18.13 (2004), pp. 2439–2454. ISSN: 1099-1085. DOI: https://doi.org/10.1002/hyp.1473. URL: https://onlinelibrary.wiley.com/doi/abs/10.1002/hyp.1473 (visited on 12/03/2020).

T. E. Lisle and M. A. Madej. "Spatial variation in armouring in a channel with high sediment supply". en. In: *Dynamics of gravel-bed rivers* (1992), pp. 277–293.

M. Luo et al. "The effect of stress history on fluctuation of bedload transport rate and bed topography in gravel-bed streams". en. In: *Journal of Hydrology* 616 (Jan. 2023), p. 128732. ISSN: 00221694. DOI: 10.1016/j.jhydrol.2022.128732. URL: https://linkinghub.elsevier.com/retrieve/pii/S0022169422013026 (visited on 06/01/2023).

L. Mao. "The effect of hydrographs on bed load transport and bed sediment spatial arrangement". en. In: *Journal of Geophysical Research: Earth Surface* 117.F3 (2012). ISSN: 2156-2202. DOI: https://doi.org/10.1029/2012JF002428. URL: https://agupubs.onlinelibrary.wiley.com/doi/abs/10.1029/2012JF002428 (visited on 11/30/2020).

Luca Mao et al. "Bedload hysteresis in a glacier-fed mountain river". en. In: *Earth Surface Processes and Landforms* 39.7 (2014). _eprint: https://onlinelibrary.wiley.com/doi/pdf/10.1002/esp.3563, pp. 964–976. ISSN: 1096-9837. DOI: https://doi.org/10.1002/esp.3563. URL: https://onlinelibrary.wiley.com/doi/abs/10.1002/esp.3563 (visited on 11/30/2020).

A. Ockelford, S. Woodcock, and H. Haynes. "The impact of inter-flood duration on non-cohesive sediment bed stability". en. In: *Earth Surface Processes and Landforms* 44.14 (2019). _eprint: https://onlinelibrary.wiley.com/doi/pdf/10.1002/esp.4713, pp. 2861–2871. ISSN: 1096-9837. DOI: 10.1002/esp.4713. URL: https://onlinelibrary.wiley.com/doi/abs/10.1002/esp.4713 (visited on 03/06/2023).

Marisa C. Palucis et al. "Intense Granular Sheetflow in Steep Streams". en. In: *Geophysical Research Letters* 45.11 (2018). _eprint: https://onlinelibrary.wiley.com/doi/pdf/10.1029/2018GL077526, pp. 5509–5517. ISSN: 1944-8007. DOI: 10.1029/2018GL077526. URL: https://onlinelibrary.wiley.com/doi/abs/10.1029/2018GL077526 (visited on 10/30/2023).

John Pitlick, Yantao Cui, and Peter Wilcock. "Manual for Computing Bed Load Transport Using BAGS (Bedload Assessment for Gravel-bed Streams) Software". In: (Jan. 2009).

I. Reid, L. E. Frostick, and J. T. Layman. "The incidence and nature of bedload transport during flood flows in coarse-grained alluvial channels". en. In: *Earth Surface Processes and Landforms* 10.1 (1985), pp. 33–44. ISSN: 1096-9837. DOI: 10.1002/esp.3290100107. URL: https://onlinelibrary.wiley.com/doi/abs/10.1002/esp.3290100107 (visited on 09/14/2021).

Dieter Rickenmann. “Hyperconcentrated Flow and Sediment Transport at Steep Slopes”. EN. In: *Journal of Hydraulic Engineering* 117.11 (Nov. 1991). Publisher: American Society of Civil Engineers, pp. 1419–1439. ISSN: 0733-9429. DOI: 10.1061/(ASCE)0733-9429(1991)117:11(1419). URL: https://ascelibrary.org/doi/10.1061/%28ASCE%290733-9429%281991%29117%3A11%281419%29 (visited on 10/30/2023).

E. J. Rindraharisaona et al. “Seismic Signature of Rain and Wind Inferred From Seismic Data”. en. In: *Earth and Space Science* 9.10 (2022). ISSN: 2333-5084. DOI: 10.1029/2022EA002328. URL: https://onlinelibrary.wiley.com/doi/abs/10.1029/2022EA002328 (visited on 12/06/2022).

D. L. Roth, E.E. Brodsky, et al. “Bed load sediment transport inferred from seismic signals near a river”. en. In: *Journal of Geophysical Research: Earth Surface* 121.4 (Apr. 2016), pp. 725–747. ISSN: 2169-9003, 2169-9011. DOI: 10.1002/2015JF003782. URL: https://onlinelibrary.wiley.com/doi/abs/10.1002/2015JF003782 (visited on 10/28/2020).

D. L. Roth, N. J. Finnegan, et al. “Bed load transport and boundary roughness changes as competing causes of hysteresis in the relationship between river discharge and seismic amplitude recorded near a steep mountain stream”. en. In: *Journal of Geophysical Research: Earth Surface* 122.5 (May 2017), pp. 1182–1200. ISSN: 21699003. DOI: 10.1002/2016JF004062. URL: http://doi.wiley.com/10.1002/2016JF004062 (visited on 11/16/2020).

B. Schmandt et al. “Multiple fluvial processes detected by riverside seismic and infrasound monitoring of a controlled flood in the Grand Canyon”. en. In: *Geophysical Research Letters* 40.18 (Sept. 2013), pp. 4858–4863. ISSN: 0094-8276, 1944-8007. DOI: 10.1002/grl.50953. URL: https://onlinelibrary.wiley.com/doi/abs/10.1002/grl.50953 (visited on 10/28/2020).

P. D. Thorne. “An overview of underwater sound generated by interparticle collisions and its application to the measurements of coarse sediment bedload transport”. en. In: *Earth Surface Dynamics* 2.2 (Dec. 2014), pp. 531–543. ISSN: 2196-632X. DOI: 10.5194/esurf-2-531-2014. URL: https://esurf.copernicus.org/articles/2/531/2014/ (visited on 10/28/2020).

V. C. Tsai et al. “A physical model for seismic noise generation from sediment transport in rivers”. en. In: *Geophysical Research Letters* 39.2 (Jan. 2012). ISSN: 00948276. DOI: 10.1029/2011GL050255. URL: http://doi.wiley.com/10.1029/2011GL050255 (visited on 10/28/2020).

J. M. Turowski, A. Badoux, and D. Rickenmann. “Start and end of bedload transport in gravel-bed streams”. en. In: *Geophysical Research Letters* 38.4 (Feb. 2011). ISSN: 00948276. DOI: 10.1029/2010GL046558. URL: http://doi.wiley.com/10.1029/2010GL046558 (visited on 10/28/2020).

J. M. Turowski, M. Böckli, et al. “Field measurements of the energy delivered to the channel bed by moving bed load and links to bedrock erosion”. en. In: *Journal of Geophysical Research: Earth Surface* 118.4 (Dec. 2013), pp. 2438–2450. ISSN: 21699003. DOI: 10.1002/2013JF002765. URL: http://doi.wiley.com/10.1002/2013JF002765 (visited on 10/28/2020).

J. M. Turowski, C. R. Wyss, and A. R. Beer. “Grain size effects on energy delivery to the streambed and links to bedrock erosion”. en. In: *Geophysical Research Letters* 42.6 (Mar. 2015), pp. 1775–1780. ISSN: 0094-8276, 1944-8007. DOI: 10.1002/2015GL063159. URL: https://onlinelibrary.wiley.com/doi/abs/10.1002/2015GL063159 (visited on 10/28/2020).

M. E. Vore et al. “Seismic Tremor Reveals Spatial Organization and Temporal Changes of Subglacial Water System”. en. In: *Journal of Geophysical Research: Earth Surface* 124.2 (2019), pp. 427–446. ISSN: 2169-9011. DOI: 10.1029/2018JF004819. URL: https://onlinelibrary.wiley.com/doi/abs/10.1029/2018JF004819 (visited on 01/23/2023).

P. R. Wilcock and J. C. Crowe. “Surface-based Transport Model for Mixed-Size Sediment”. en. In: *Journal of Hydraulic Engineering* 129.2 (Feb. 2003), pp. 120–128. ISSN: 0733-9429, 1943-7900. DOI: 10.1061/(ASCE)0733-9429(2003)129:2(120). URL: http://ascelibrary.org/doi/10.1061/%28ASCE%290733-9429%282003%29129%3A2%28120%29 (visited on 07/01/2021).

W. S. D. Wilcock, S. C. Webb, and I. Th. Bjarnason. “The effect of local wind on seismic noise near 1 Hz at the MELT site and in iceland”. In: *Bulletin of the Seismological Society of America* 89.6 (Dec. 1999), pp. 1543–1557. ISSN: 0037-1106. DOI: 10.1785/BSSA0890061543. URL: https://doi.org/10.1785/BSSA0890061543 (visited on 03/20/2023).

M. Gordon Wolman. “A method of sampling coarse river-bed material”. en. In: *Eos, Transactions American Geophysical Union* 35.6 (1954). _eprint: https://onlinelibrary.wiley.com/doi/pdf/10.1029/TR035i006p0 pp. 951–956. ISSN: 2324-9250. DOI: 10.1029/TR035i006p00951. URL: https://onlinelibrary.wiley.com/doi/abs/10.1029/TR035i006p00951 (visited on 10/20/2023).

Audio 1: Hydrophone audio recording during the water level peak of the September-October event showing the lower frequency signals observed in the hydroacoustic data, attributed to larger grains being transported.

Audio 2: Hydrophone audio recording showing the higher frequency signals recorded at water levels below approximately 1.6 m during the September-October event which were categorised as the movement of smaller particles.

Audio 3: Hydrophone audio recording during of the background turbulence signal following the cessation of bedload transport during the September-October event.

Sounding Out The River: Seismic and Hydroacoustic monitoring of bedload transport in an alluvial river - Supplemental Material

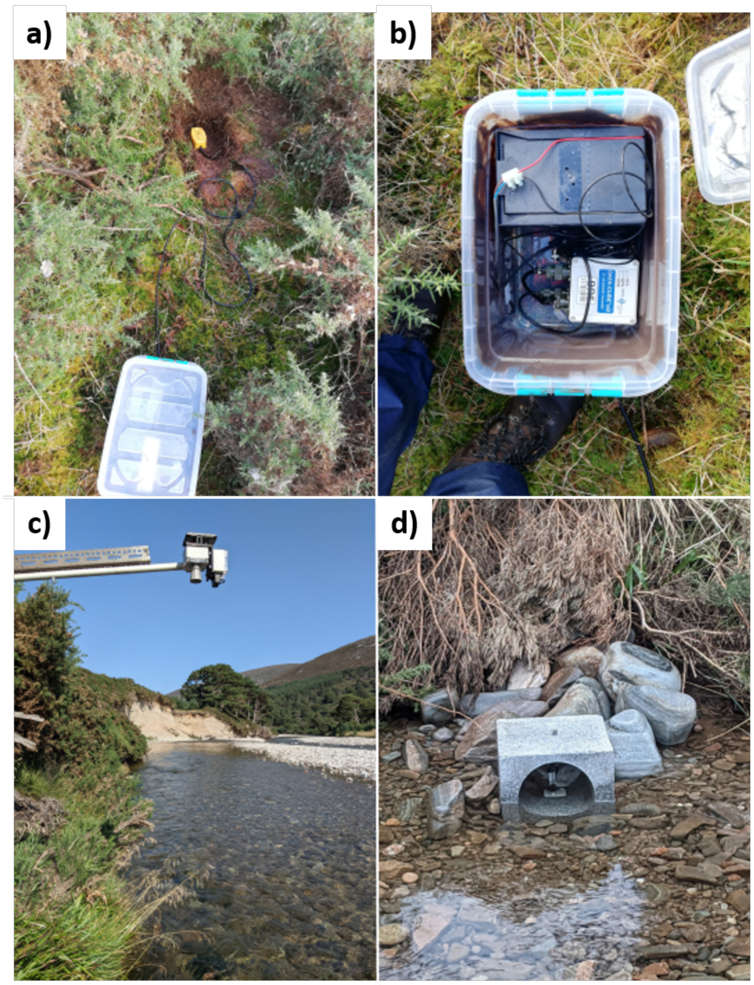

S1: Images of the field deployed instruments.(a, b) Seismic sensor setup with geophone buried on shallow soil connected to a datalogger and battery, (c) water level sensor SG2, (d) hydrophone setup at site W_07.

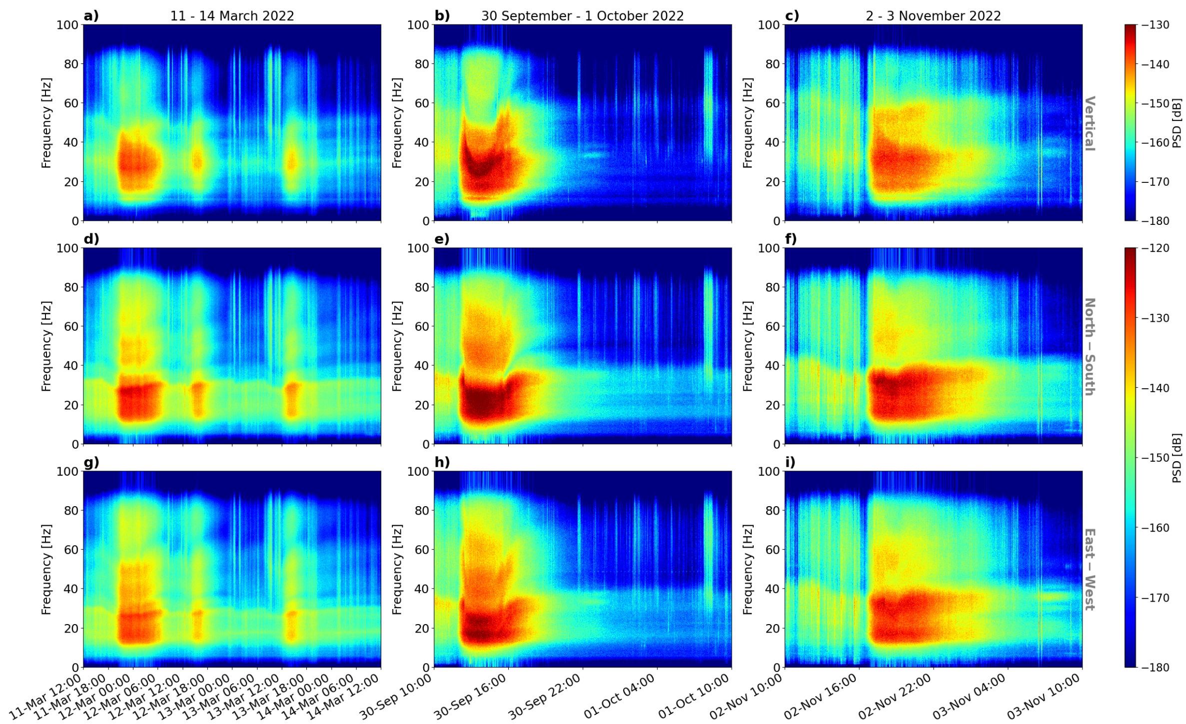

S2: Spectrograms for each of the three events (columns) for each of the three geophone components (rows) demonstrating the similarity in information for all three components, but highlighting the less distinct river-induced signal in the vertical component (a, b, c) therefore resulting in a greater influence from the rain signals prior to the flood wave.

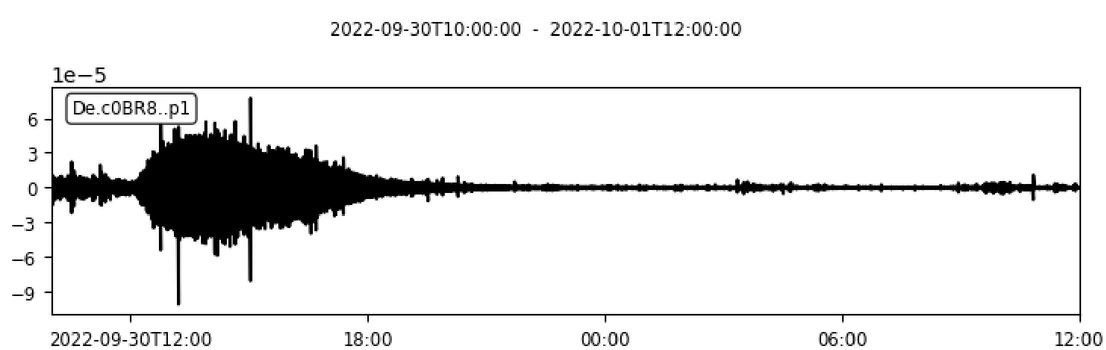

S3: Waveform of the north-south component at site W_07 during the September-October event demonstrating the saturation in the PSD at high water levels is not because of clipping of the waveforms.

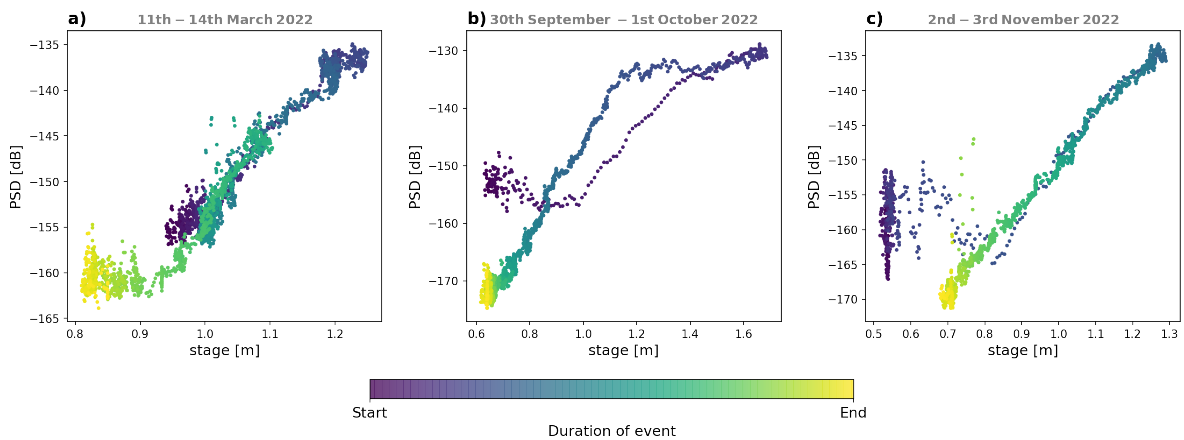

S4: SG2 water level versus PSD over 20-30 Hz for the north-south component at site W_07 for all three events. This reveals a similar behaviour to the higher frequency band in Figure 3.